IOP Publishing Measurement Science and Technology
Meas. Sci. Technol. **31** (2020) 055102 (12pp) https://doi.org/10.1088/1361-6501/ab63ea

# Real-time sitting behavior tracking and analysis for rectification of sitting habits by strain sensor-based flexible data bands

**Yangyang Zhang[1], Ying Huang[1,2,4,5], Baisheng Lu[1], Yuanming Ma[1], Jihong Qiu[1], Yunong Zhao[1], Xiaohui Guo[3], Caixia Liu[1], Ping Liu[1] and Yugang Zhang[1]**

[1] School of Electronic Science and Applied Physics, Hefei University of Technology, Hefei 230009, People's Republic of China
[2] The State Key Laboratory of Bioelectronics, Southeast University, 210096, People's Republic of China
[3] School of Electronics and Information Engineering, Anhui University, Hefei 230601, People's Republic of China

E-mail: hf.hy@163.com

Received 3 October 2019, revised 14 December 2019
Accepted for publication 19 December 2019
Published 6 February 2020

**Abstract**

From human–machine interfaces to human–computer/robot interaction, the prevailing pattern has gradually become one of people remaining in a sitting posture while working. However, unhealthy sitting behavior seriously affects human health. This paper presents a novel tracking and analysis method of real-time sitting behavior. It is designed using a series of flexible wearable data bands, based on flexible stretchable sensors and pressure sensors (PSNRs). A flexible PSNR is fabricated using composites of carbon black, carbon nanotubes and silicon rubber, by a mixed solution method; it possesses a good property of pressure perception, for tracking sitting behavior. The sensors are accurately attached to human joints for accurate measurement of joint movement at the shoulders, elbows, wrists, knees, and waist. In this work, a new idea of real-time sitting behavior recognition is introduced and developed, based on a radial basis function neural network. Dynamic time warping is used to select candidates for dynamic sitting behavior and also to recognize postures by comparing the observed records with a series of pre-recorded reference data patterns. The solution deals simultaneously with real-time sitting behaviors as well as with multiple joints within the area of interest, to monitor the health level of the sitting behavior and to remind humans of sitting habits. The experimental results of the real-time sitting behavior tracking and analysis verify the effectiveness of the proposed methods. Additionally, undesirable sitting behaviors were gradually rectified and the sitting habit health levels of the participants were gradually increased.

Keywords: strain sensor, wearable data band, sitting habit, real-time posture analysis

S Supplementary material for this article is available online

(Some figures may appear in colour only in the online journal)

[4] Author to whom any correspondence should be addressed.
[5] School of Electronic Science and Applied Physics, Hefei University of Technology, NO. 193 Tunxi Road, Hefei, Anhui, People's Republic of China

 

## 1. Introduction

From human–machine interfaces (HMIs) to human–computer/robot interaction (HCI/HRI), the working pattern of a human in a sitting posture has gradually become a prevailing pattern of human work and life. However, unhealthy sitting behaviors seriously affect people's health [1–3], producing problems such as myopia [4], cervical spondylopathy [5], poor circulation [6], humpback [7], spondylitis [8], and protrusion of the lumbar intervertebral disc [9]. This justifies the interest of the research community in the development and advancement of sitting behavior tracking and analysis technologies. However, this is a daunting task. As it is very hard to accurately detect sitting behavior in an unpredictable environment, the problem is both complex and limited. Various posture tracking and recognition approaches have been proposed. The existing research can be divided into two categories: vision-based or wearable sensors-based [10–12]. Vision-based technologies use image processing to extract useful information. Technologies based on wearable sensors depend on physical interaction with the users. The vision-based methods are always easily affected by environmental factors such as occlusion, illumination, and the positioning of the equipment [13]. In contrast, wearable sensor-based technologies are easy to implement and can usually provide more reliable behavior information [14–16]. Accurate and real-time posture acquisition and recognition algorithms occupy a very important position in major research areas [17, 18]. In the analysis of sitting behavior, there are generally two challenges. One challenge is in the choice of appropriate features to represent the behavior. This problem is very difficult due to the specific flexibility and randomness of human limbs [19]. The other challenge concerns the adoption of proper analysis procedures to correctly recognize the postures [20].

With the rapid development of artificial intelligence technologies, the fusion of smart data feature information has gradually become a mature technology. Flexible sensors have acquired the advantages of low power consumption, good extension, small size, and good wearability [21, 22]. Additionally, flexible strain sensors have been proven to be a good method of measuring human motion performance [23, 24]. Compared to research using a visual system, flexible strain sensors show a higher dexterity and correlation. A textile-based sensing system has been presented [25] which analyzes the sitting posture accurately and non-invasively. Several effective techniques have been proposed to improve the recognition rate of sitting postures, including sensor calibration and dynamic time warping (DTW)-based classification. One study developed models to detect proper and improper sitting postures [26], using gyroscope readings through mobile devices. The models were developed by training classifiers of the *k*-nearest neighbor, a support vector machine (SVM), and multi-layer perception. An approach using an accelerometer sensor [27] was presented for activity recognition. The resulting feature vector is further processed using linear-discriminant analysis and artificial neural networks to recognize a particular human activity. A method was proposed to recognize complex daily activities which consist of simultaneous body activities in an indoor environment [28]. Three motion sensor nodes are attached to the right thigh, the waist, and the right hand. A method [29] of recognizing muscular activities was proposed, using air pressure sensors and air bladders. The muscular activity is detected by measuring the change of air pressure in an air bladder that contacts the muscles of interest. Another study [30] addressed natural HRI in a smart assisted living system for the elderly and the disabled. For gesture recognition, they implemented a neural network for gesture spotting and hierarchical hidden Markov models for context-based recognition. For daily activity recognition, a multi-sensor fusion scheme was developed to process motion data collected from the foot and the waist. A wearable, gesture-based controller was fabricated [31], using the sensing capabilities of flexible thin-film piezoelectric polymer polyvinylidene fluoride (PVDF). Forearm muscle movements were detected by the PVDF, which sent its voltage signals to a developed microcontroller-based board. They were then processed by an artificial neural network that was trained to recognize the generated voltage profile of gestures. The principal component analysis method and a generalized regression neural network were used to construct a gesture recognition system [32], so as to reduce the redundant information of electromyography signals, improve the recognition accuracy, and enhance the feasibility of real-time recognition. It was found that due to the high coupling of electromyography signals, accurate gesture recognition was difficult to achieve. A novel multi-sensor system [33] was proposed for accurate dynamic hand gesture recognition. It employed convolutional deep neural networks to fuse data from multiple sensors and to classify the gestures.

The research shows that there are still some challenges [34, 36] in the study of real-time human behavior tracking and analysis, including sitting behaviors based on wearable equipment [37]. These problems are as follows: (i) the development of reliable properties of wearability and sensitivity in devices that minimize the discomfort or embarrassment of the patient; (ii) the problem of inconsistency in time series of dynamic behaviors; and (iii) the lack of accurate and appropriate methods of posture recognition. This work addresses these problems and develops a novel, flexible wearable data band based on stretchable sensors and pressure sensors that offers reliable wearability and sensitivity and minimizes the discomfort or embarrassment of users [38–40] (Extended Data table 1, supplementary video (stacks.iop.org/MST/31/055102/mmedia)). Since technologies based on wearable data bands depend on physical interaction with the users, the data bands developed have body sensor networks to ensure that the sensors are accurately attached to the human joints for accurate measurement of joints movement at the shoulders, elbows, wrists, knees, and waist. As such, they can provide more reliable behavior

**Table 1.** Static sitting posture recognition accuracy of different approaches.

| Approaches | RBFNN | SVM | RBFNN-Kernel | SVM-Kernel |
|---|---|---|---|---|
| Accuracy (%) | 90.92 | 89.85 | 94.25 | 90.20 |
| Training time (s) | 6.25 | 35.97 | 16.33 | 89.55 |


**Figure 1.** The proposed wearable data bands system.

information on static and dynamic sitting postures. Finally, appropriate sitting behavior recognition methods with good generalization ability are proposed.

Various classification methods have been applied to pattern recognition, such as the *k*-nearest neighbor, an artificial neural network, and the SVM [41, 42]. Nonetheless, it is known that all of them face some challenging issues, such as slow training speed, trivial human intervention, large computational requirements, and poor generalization ability. Compared with those methods, RBFNN always handles the hard-to-analyze regularity in the system. In addition, it has good performance in generalization ability and has been successfully applied to time series analysis, pattern recognition, and system construction [43]. Furthermore, the DTW algorithm is used to select behavior candidates and to recognize postures when combined with RBFNN by comparing an observed posture with a series of pre-recorded reference patterns, and to solve the problem of inconsistency in time series in real-time dynamic sitting behavior recognition.

The remainder of this paper is organized as follows. The real-time sitting behavior tracking and acquisition methods are introduced in section 2. Section 3 presents the theories of real-time sitting behavior recognition and analysis algorithms built on methods based on RBFNN-DTW. Section 4 gives the experimental results, and section 5 presents the conclusion of this work.

## 2. The architecture of the proposed system

In this section, the real-time sitting posture tracking method is presented. First, the flexible wearable data band design methods are presented, followed by the development of the sitting behavior tracking and analysis algorithms.

### 2.1. Design of pressure sensor

*2.1.1. Materials.* The carbon black (CB) used in this study was CB-3100, which exhibits an average particle size of 30 nm, and is produced by the Swiss SPC chemical company. The single-walled carbon nanotubes (SWCNTs) powder was purchased from Chengdu Organic Chemicals Co. Ltd. The mean length and diameter of the SWCNTs are 20 mm and 2 nm, respectively. The polystyrene sulfonate (PSS) was purchased from Shanghai Mackin Biochemical Co., Ltd. The samples' matrix silicon rubber (SR) (SR-GD401) was provided by Sichuan Zigong Chenguang Chemical Institute. Conductive silver (YC-02) paste was purchased from Nanjing Hang Shuo Electronic Technology Co., Ltd.

*2.1.2. Fabrication of pressure sensor.* For pressure sensors used in human wearable equipment, flexibility is especially necessary. In the first step in the preparation of the sensitive materials, 0.20 g of CB and 0.14 g of SWCNTs were homogeneously dispersed in a naphtha solution. This was followed with sonication for 1 h and magnetic stirring for 6 h. Next, 2.6 g of SR was homogeneously dispersed in the CB/SWCNTs composite solution with magnetic stirring for 3 h. After that, the resulting composite solution was spin-coated to form a film and places in a thermostatic drying oven foaming at 60 °C for 30 min. Subsequently, the solid composites were left to dry completely at room temperature for 24 h. Finally, the mixture was precisely tailored and cut into a unit and the electrodes of conductive silver paste were covered on the sensor array for 2 d to complete the curing process and bring them into close contact, as shown in the Extended Data, figure 1.

### 2.2. Wearable data bands design, and posture acquisition

The proposed fully flexible data bands have two types of strain sensors: pressure sensors and stretchable sensors. The stretchable sensors used here were proposed in the authors' previous studies [44], in which a highly stretchable fiber-based sensor was fabricated. The stretchable sensors have the capacity to detect and monitor motions in human joints and skin, and are more flexible, more comfortable and more dexterous than traditional sensors. Additionally, the stretchable sensors exhibited good sensibility and rapid response.

The wireless transmission modules of the CC-2530 were used to process the basic data and evaluate results, encapsulating them into packets and sending the packets to the computation center. The baud rate of data transmission is 115 200 bps, and the frequency reaches 50 Hz. The architecture of the proposed wearable data bands is shown in figure 1. The architecture of the proposed sitting behavior tracking and analysis system is shown in figure 2. Two assumptions are made about the participants in the experiments: (i) the body structures of the participants are symmetrical; and (ii) the sitting postures of the participants are homologous to those of the broad masses of the people. Therefore, based on the wearable data bands, sitting behavior can be conveniently estimated.

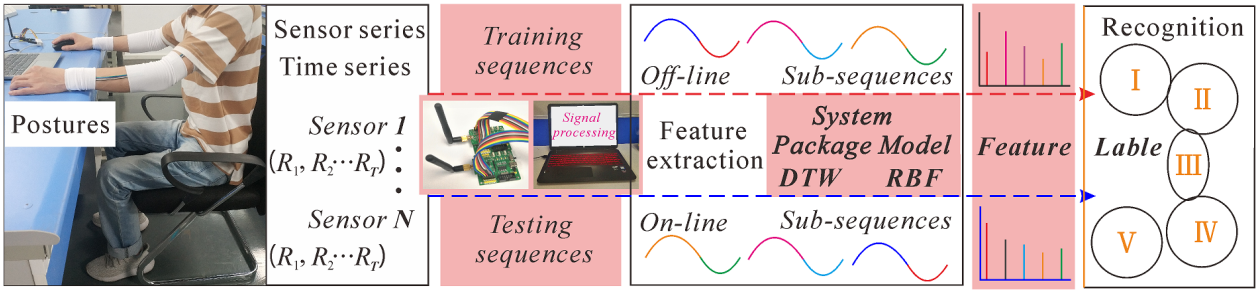


**Figure 2.** The architecture of the proposed sitting behavior tracking and analysis system.

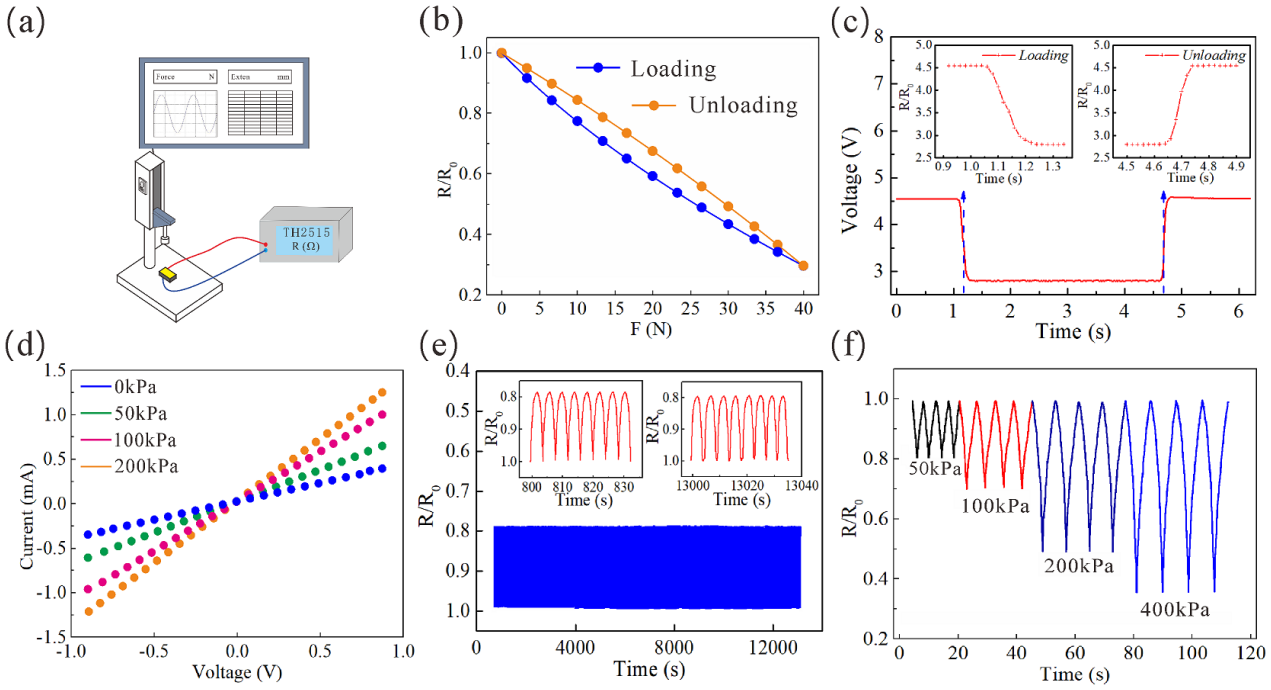


**Figure 3.** (a) The pressure test platform. (b) Relative resistance changes under applied pressure of loading and unloading. (c) Relaxation times of the pressure sensor. (d) Current–voltage curves of the pressure sensor under different pressures. (e) Durability test during 12 000 loading/unloading cycles. Insets: magnified diagram of the selected areas. (f) The pressure sensor response to dynamic loading/unloading cycles at various pressures.

## 3. Human real-time sitting posture recognition

In this section, the real-time static and dynamic sitting postures recognition methods are proposed. The framework of the system is presented, and the real-time sitting behavior analysis method based on RBFNN-DTW is described.

### *3.1. Architecture of sitting posture recognition*

The recognition of sitting behavior by using the proposed wearable data bands is divided into three stages. The first stage is to establish databases of sitting postures. First, the data of various sitting postures are collected through the proposed wearable data bands. The datasets which include static sitting postures and dynamic sitting postures are then established. The second stage is to train the classifiers. On the basis of the datasets, the features of each sitting posture are extracted and expressed. The final stage is experiment and analysis. The sitting posture data of various sitting behaviors from various participants are collected, and the trained classifiers are used for real-time posture recognition. The architecture of the proposed system is shown in the Extended Data, figure 2.

### *3.2. Static sitting posture recognition*

RBF was first proposed by Broomhead and Lowe in 1988, and stemmed from Powell's seminal research from 1977 [45]. RBF is a real-valued function whose value depends on the distance from the origin; it can also be interpreted as a simple kind of neural network. RBF is also used as a kernel in classification and is sufficiently ready to have the RBFNNs exploited in various applications. The model of the RBFNN is shown in the Extended Data, figure 3.

Suppose the input data $\boldsymbol{X}$, $\boldsymbol{Y}$ is the classification results of the output. We can then obtain the output framework of the model as

$$Y = F(X). \tag{1}$$

The input data is $\boldsymbol{X} = (x_1, x_1, \ldots, x_L)$, and $\varphi_i(X)$ denotes the hidden nodes' nonlinear, piecewise and continuous activation functions. The output functions of $N$ hidden layer nodes can then be described as

$$F(X) = \omega_0 + \sum_{i=1}^{N} \omega_i \varphi_i(x_i - x_c). \tag{2}$$

Here, $N$ is the dimension of input data, $\omega_i$ denotes the output weight vectors of the node from the $i$th hidden layer, and $x_c$ is the activation function center.

According to the theory of Bartlett [46], the method due to the least weight is used to calculate the output weights, and the minimum error solution through the minimum norm can be obtained by RBFNN, which achieves good general properties. For specified training samples $(x_i, t_i)$, the output of $N$ hidden layer nodes can be described using

$$f(x) = \omega_0 + \sum_{i=1}^{N} \omega_n \varphi_n(\|x - c_i\|) = \boldsymbol{\omega} \cdot \boldsymbol{\Phi}(x) \tag{3}$$

$$\boldsymbol{\Phi} \cdot \boldsymbol{\omega} = T \tag{4}$$

$$\boldsymbol{\Phi} = \begin{pmatrix} \varphi_1(\varepsilon_1, x_1) & \cdots & \varphi_N(\varepsilon_L, x_1) \\ \vdots & \cdots & \vdots \\ \varphi_1(\varepsilon_1, x_L) & \cdots & \varphi_N(\varepsilon_L, x_1) \end{pmatrix} \tag{5}$$

$$\boldsymbol{\omega} = [\omega_0, \omega_1, \ldots, \omega_L] \tag{6}$$

$$T = \begin{bmatrix} t_1^{\mathrm{T}} \\ \vdots \\ t_L^{\mathrm{T}} \end{bmatrix}_{L \times d}. \tag{7}$$

According to the input $x_i$, the network matrix $\Phi$ denotes the outputs of hidden layers, and the $i$th row represents the output vector of the hidden layer. According to all input $(x_1, ..., x_L)$, the $i$th column represents the output of the $i$th hidden layer neuron. The minimum norm of the least-square solution of the linear system can be described using one of the two following expressions:

$$|\boldsymbol{\Phi} \cdot \hat{\boldsymbol{\omega}} - T| = \min_{\omega} |\boldsymbol{\Phi} \cdot \omega - T| \tag{8}$$

$$\hat{\boldsymbol{\omega}} = \boldsymbol{\Phi}^{\dagger} T. \tag{9}$$

In (9), $\Phi^{\dagger}$ denotes the Moore–Penrose generalized inverse of the network matrix. In order to improve the generalization ability of RBF as compared to the RBFNN based on the least square solution, it was necessary to generate the input weights randomly. Kernel methods were used in designing the RBF, and a positive value parameter $C^{-1}$, defined by the users, is proposed for the calculation of the output weights in (10):

$$\omega = \boldsymbol{\Phi}^{T}(C^{-1} + \boldsymbol{\Phi}\boldsymbol{\Phi}^{T})T. \tag{10}$$

The kernel-based RBF can then be expressed as

$$K_{\mathrm{RBF}}(x_i, x_j) = \boldsymbol{\Phi}(x_i)\boldsymbol{\Phi}(x_j) = [f(\omega_1, \sigma, x_i), \ldots, f(\omega_N, \sigma, x_i)]^{T} \cdot [f(\omega_1, \sigma, x_j), \ldots, f(\omega_N, \sigma, x_j)]^{T}. \tag{11}$$

Due to the parameters of $(w, \sigma)$ being randomly assigned, an optimization model of the dual kernel optimization function is formed as follows. Minimize

$$L_D = \tfrac{1}{2} \sum_{i=1}^{N} \sum_{j}^{N} t_i t_j K_{\mathrm{RBF}}(x_i, x_j) \alpha_i \alpha_j - \sum_{i=1}^{N} \alpha_i \quad 0 \leqslant \alpha_i \leqslant C, \quad i = 1, \ldots, N. \tag{12}$$

Referring to '(13)–(16)', the regularized RBFNN is selected, and when the Gaussian function is chosen as the basis function of the neural network, the connection weights of neurons between the hidden layers and the output layers are calculated by the least squares method:

$$\varphi(x) = \mathrm{e}^{-\frac{1}{2\sigma^2}x^2} \tag{13}$$

$$F(x) = \sum_{i=1}^{N} \omega_i \mathrm{e}^{-\frac{1}{2\sigma^2}||x - x_i||^2} \tag{14}$$

$$\sigma_i = {}^{c_{\max}}\!\!\diagup_{\sqrt{2h}} \tag{15}$$

$$\omega = \exp(hc^{-2}{}_{\max}||x_p - c_i||^2). \tag{16}$$

The RBF kernel is the result of a combination of nuclear learning optimization and standard methods to find the optimal solution. As the optimization constraints are slight, the RBF kernel achieves better generalization performance.

### 3.3. Real-time dynamic sitting behavior recognition

Real-time sitting behaviors involve inconsistent action sequences, so the time series characteristics of the collected samples are not consistent. A dynamic programming algorithm is used to search for optimal matching between the two sequences, defining the distance measure of the two sequences, which is used to solve the inconsistency. The DTW technique is used to address the problems of human real-time sitting postures. The DTW algorithm establishes a scientific time alignment, matching the path between the features of the test patterns and the reference patterns. In time series, the features of two time series which must be comparatively similar are always inconsistent. In the matter of real-time sitting posture recognition, the frequency of actions and the random characteristics of people differ; even if the same person repeats the same behavior, it is impossible to reproduce the coincident time series. The traditional Euclidean distance methods are not very effective in calculating the distance between two time series in these complex cases (Extended Data, figures 4(a) and (d)). The solid line and the dashed line are two waveforms

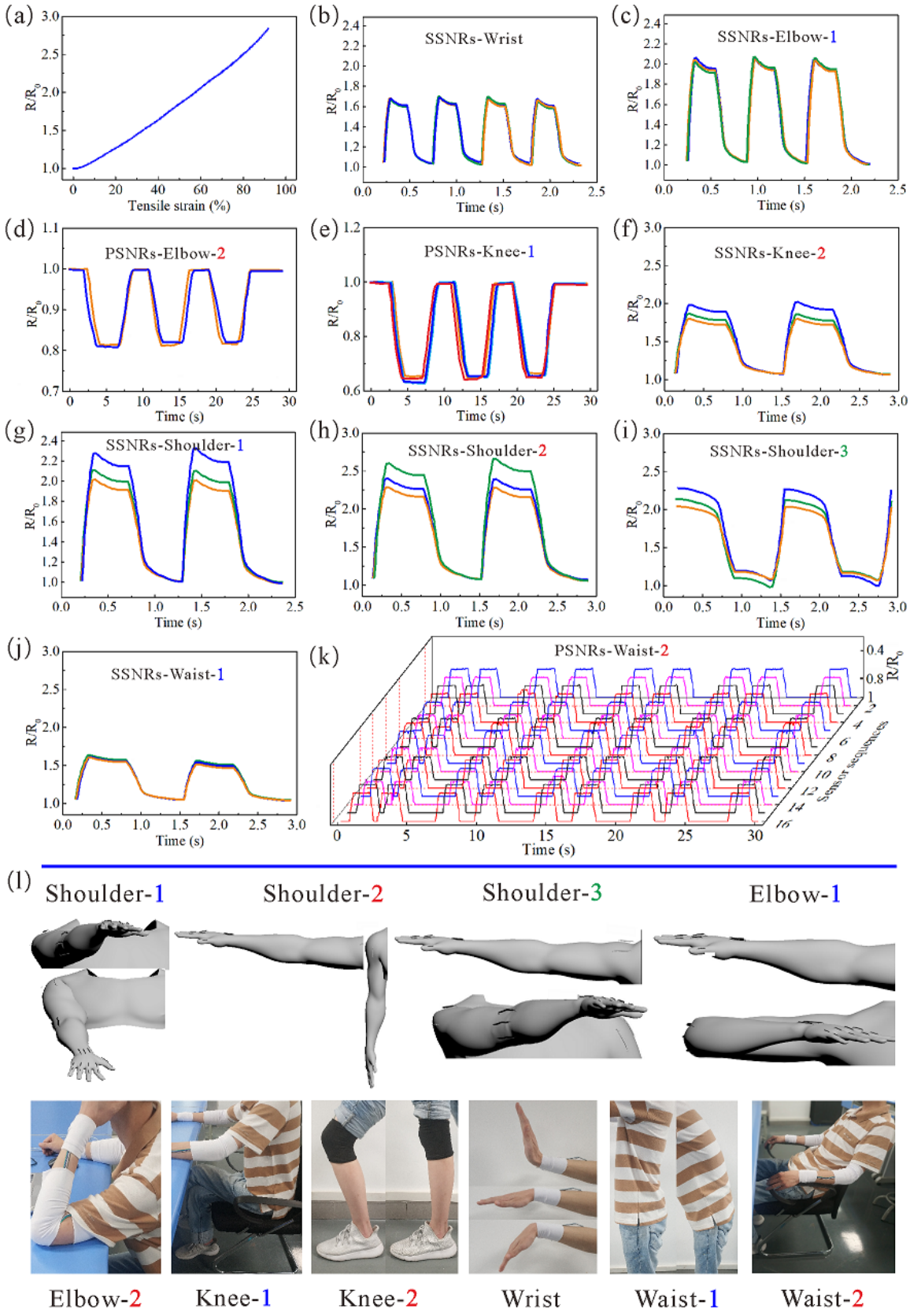


**Figure 4.** Typical response curves of strain sensors induced by sitting behaviors. (a) Relative resistance changes of the SSNR under 100% strain level. The typical relative resistance changes due to (b) wrist joint actions (SSNRs), (c) elbow joint action-1 (SSNRs), (d) elbow joint action-2, (e) knee joint action-1 (PSNRs), (f) knee joint action-2 (SSNRs), (g) shoulder joint action-1 (SSNRs), (h) shoulder joint action-2 (SSNRs), (i) shoulder joint action-3 (SSNRs), (j) waist action-1 (SSNRs), (k) waist action-2 (PSNRs), and (l) various cases of typical human joint actions.

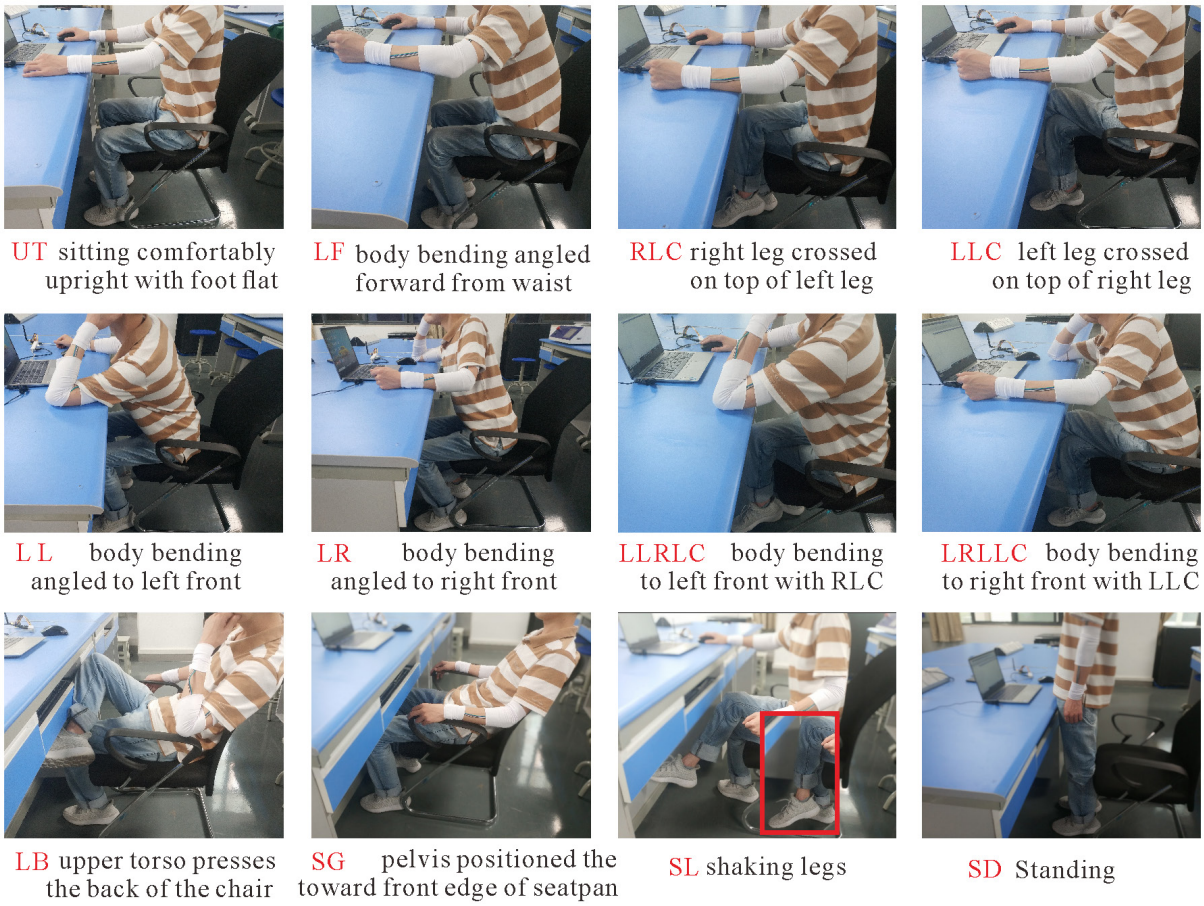


**Figure 5.** Typical sitting behaviors.

of the same behavior. It can be seen that the overall waveforms are very similar but inconsistent on the time axis. The point '*a*' of the real line waveform corresponds to point '*b*' of the dashed line waveform. The traditional method calculates the similarity by comparing the distance, which is obviously unreliable because it is evident that point '*a*' of the solid line corresponds to point '*b*' of the dashed line (Extended Data, figure 4(e)).

Suppose we have two experimental time series, $\boldsymbol{R}_i$ and $\boldsymbol{R}_j$. Suppose that $\boldsymbol{R}_i = (r_1, r_2, \ldots, r_i)$ are the test pattern features vector sequences, and $\boldsymbol{R}_j = (r_1, r_2, \ldots, r_j)$ are the reference pattern features vector sequences, and $i$, $j$ represent the time serial number. Then

$$\boldsymbol{P}(\boldsymbol{R}^T) = [P_1(R^1)...P_1(R^T), ..., P_N(R^1)...P_N(R^T)]. \quad (17)$$

The time feature space is formed by splicing outputs with the time window under a unified time thread $\boldsymbol{P}$ in time $T$ quantum, and $N$ is the serial number of the sensors, as shown in (17).

A warping path $\boldsymbol{W}$ is used to define a mapping between $R_i$ and $R_j$, where $\boldsymbol{W} = (w_1, w_2, \ldots, w_k, \ldots, w_K)$, $\max(i, j) \leqslant K \leqslant i + j - 1$. The variable $K$ represents the final warping path, and $w_k = (i, j)_k$ is the $k$th mapping gain between the $i$th test experimental pattern feature vector and the $j$th reference pattern feature vector. The warping path searching process of the time series, between the test pattern and reference pattern features vector sequences, is shown in the Extended Data, figure 4(f).

This limits the point of $\boldsymbol{W}$ to be monotonous over time. Therefore, the minimizing warping function can be described as

$$\mathrm{DTW}(R_i, R_j) = \min(K^{-1}\sqrt{\sum_{n=1}^{N} w_n}), \quad (18)$$

and the path can be found using the dynamic programming method to evaluate the recurrence that defines the accumulative distance $L(R_i, R_j)$ and the present kernel distance $N(R_i, R_j)$:

$$L(R_i, R_j) = N(R_i, R_j) + \min\{L(R_i - 1, R_j - 1), L(R_i - 1, R_j), L(R_i, R_j - 1)\}. \quad (19)$$

Therefore, the functions of the RBFNN kernel can be described as

$$K(x, x_i) = \exp(-\lambda||x, x_i||^2). \quad (20)$$

Currently, the methods of combining DTW and the RBF kernel to achieve the purpose of real-time sitting posture recognition according to the analyzed time series can be described as

| | UT | LF | LL | LR | RLC | LLC | LLRLC | LRLLC | LB | SG | SL | SD | Total | Recall |
|---|---|---|---|---|---|---|---|---|---|---|---|---|---|---|
| UT | 92 | 3 | 0 | 0 | 0 | 0 | 0 | 0 | 1 | 2 | 0 | 0 | 100 | 2 |
| LF | 2 | 93 | 0 | 0 | 0 | 0 | 0 | 0 | 0 | 2 | 0 | 0 | 100 | 3 |
| LL | 0 | 0 | 93 | 0 | 0 | 0 | 0 | 0 | 2 | 3 | 0 | 0 | 100 | 2 |
| LR | 0 | 0 | 0 | 95 | 0 | 0 | 0 | 0 | 2 | 2 | 0 | 0 | 100 | 1 |
| RLC | 0 | 0 | 0 | 0 | 96 | 0 | 2 | 0 | 0 | 0 | 0 | 0 | 100 | 2 |
| LLC | 0 | 0 | 0 | 0 | 0 | 95 | 0 | 2 | 0 | 0 | 0 | 0 | 100 | 3 |
| LLRLC | 0 | 0 | 0 | 0 | 2 | 0 | 92 | 0 | 0 | 0 | 3 | 0 | 100 | 3 |
| LRLLC | 0 | 0 | 0 | 0 | 2 | 0 | 0 | 93 | 0 | 0 | 4 | 0 | 100 | 1 |
| LB | 1 | 0 | 2 | 2 | 0 | 0 | 0 | 0 | 94 | 0 | 0 | 0 | 100 | 1 |
| SG | 2 | 3 | 2 | 2 | 0 | 0 | 0 | 0 | 0 | 90 | 0 | 0 | 100 | 1 |
| SL | 0 | 0 | 0 | 0 | 0 | 0 | 3 | 3 | 0 | 0 | 92 | 0 | 100 | 2 |
| SD | 0 | 0 | 0 | 0 | 0 | 0 | 0 | 0 | 0 | 0 | 0 | 98 | 100 | 2 |

**Figure 6.** Typical static sitting posture recognition accuracy for the RBFNN approach.

$$K(R_i, R_i) = \exp[-\lambda DTW(R_i, R_i)^2], \tag{21}$$

where $\lambda$ denotes the prescribed adjustment parameter.

In order to monitor the health level of the sitting habit, the health level parameter *HL* is defined. Assuming that the total time in the *i*th monitoring period is $T$, and the time window of the single sitting behavior is $t$, the total number of sitting postures of the *i*th monitoring period is $T_i/t_i$. The sitting habit health level of the *i*th monitoring period is defined by

$$HL(T_i, t_i) = n(t_i)/N(T_i), \tag{22}$$

where $n$ is the number of healthy sitting behaviors, and $N$ is the total number for the *i*th monitoring period. Therefore, the health level *HL* of the sitting habit of all of the participants is defined as

$$HL(T, t) = (\sum_{i=1}^{N} t_i)/(\sum_{i=1}^{N} T_i). \tag{23}$$

The sitting postures used here are representative of the typical sitting postures that can be found in life and at work [47, 48].

## 4. Experiments and results

The experiments in the following sections focus on the contributions of this paper, the sitting behavior tracking method, and the sitting behavior analysis method based on RBFNN-DTW.

### *4.1. Pressure sensor performance*

The piezoresistive properties testing platform is illustrated in figure 3(a). The response curve and typical hysteresis response curve during loading and unloading pressure of the sensor are shown in figure 3(b). The stretchable sensors and pressure sensors used here both have hysteresis characteristics. As the monitoring process of sitting behavior is dynamic, the training pattern sets characteristics and the testing pattern sets all contain the hysteresis information of the sensors. In the procedure of sitting behavior classification and analysis, the hysteresis characteristics of the sensors are firmly transformed into available features information. Therefore, the DTW-based dynamic information processing methods exclude the influence of the hysteresis characteristics on the accuracy of the sitting behavior tracking and analysis.

In addition, the system displayed rapid response and recovery properties, defined as the time taken to achieve 90% of the total voltage change, of 110 ms and 120 ms respectively (figure 3(c)). Next, the device stability was investigated by a periodic loading and releasing process. Depending on the static mechanical pressure, the sensor registered an increase in electrical current based on current–voltage curves, indicating successful detection of static mechanical pressures (figure 3(d)). The stability and repeatability of the sensor was further tested by periodic loading and unloading cycles, as demonstrated in figure 3(e). It can be seen that after 12 000 cycles, it still exhibited good stability with around a 20% change (based on the highest resistance), together with mechanical reliability and long-term durability. The resistance change of the sensor under different strains was monitored in the process of cyclic loading and releasing, demonstrating the dynamic characteristic of the device. Figure 3(f) records the dynamic relative resistance change ($R/R_0$) during several loading and releasing cycles, and no disparate change tendency or evident drift was found, showing the prominent flexibility and repeatability under various strains, where $R$ and $R_0$ are the resistances before and after applying strain, respectively.

### *4.2. Sitting behavior tracking experiments*

With the purpose of making the developed data bands truly useful in a real-world environment, we investigated their thermal and humidity stability by showing the response of the materials as a function of temperature and humidity (Extended Data, figure 5) [49–53].

As shown in figure 4, the normalized initial resistance of the stretchable sensors was set to be the resistance values of the sensors in a non-strain state. The movements of the shoulder joints, elbow joints, wrist joints, knees, and the waist

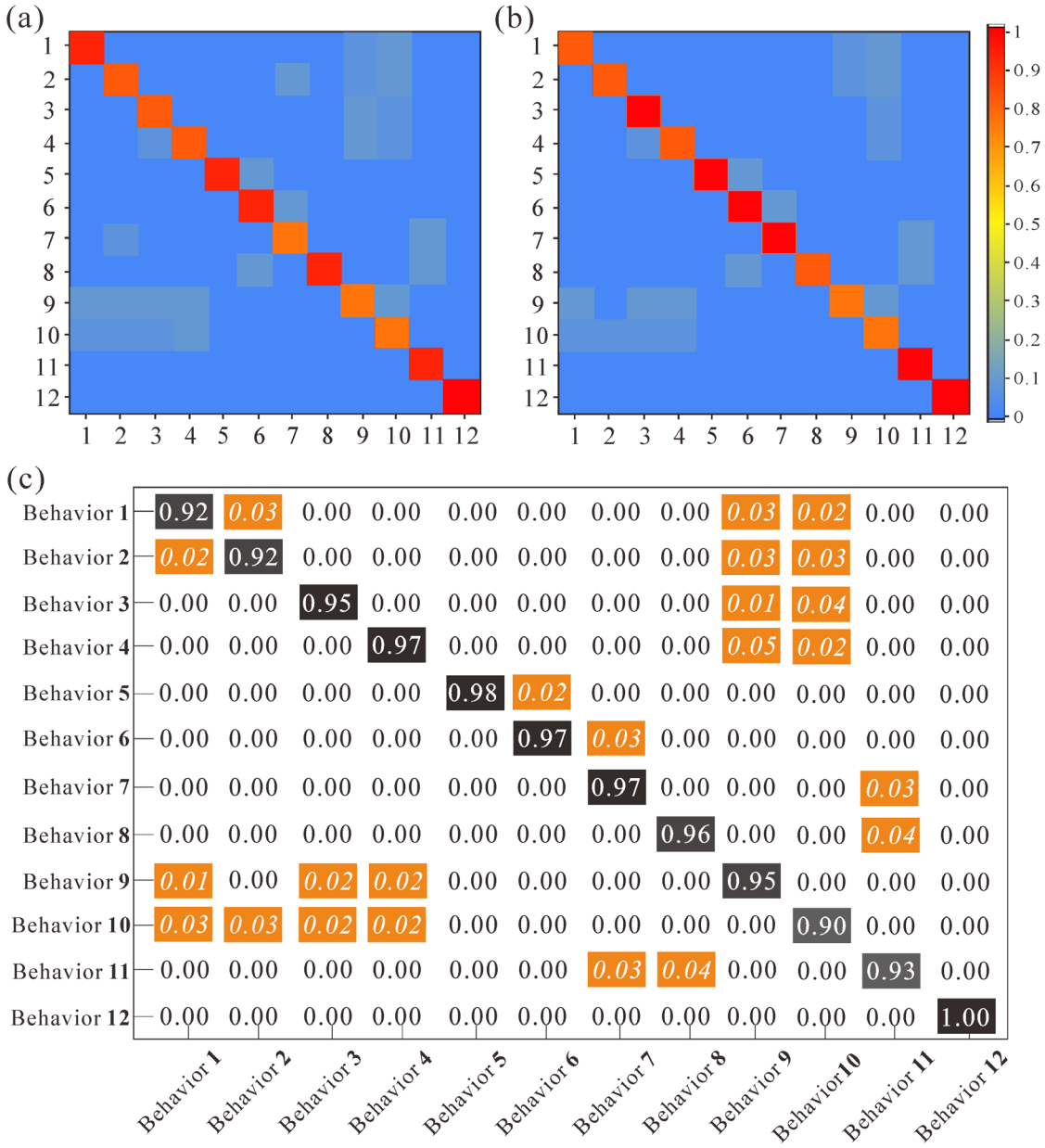


**Figure 7.** The confusion matrix across 12 sitting behaviors using (a) RBF, (b) SVM-Kernel-DTW, and (c) RBF-Kernel-DTW.

can easily be captured and distinguished. Furthermore, the recognition accuracy of the results can be evaluated using statistical techniques.

### *4.3. Sitting behavior recognition and analysis experiments*

*4.3.1. Static sitting behavior recognition experiments.* The sitting behavior recognition was verified based on a series of experiments which verify the validity of RBFNN-based recognition methods. As a basis for the experiments, a dataset was recorded containing 12 categories of sitting postures. The postures contained in the database are as follows: upright (UT), leaning forward (LF), leaning left (LL), leaning right (LR), right leg crossed (RLC), left leg crossed (LLC), leaning left with right leg crossed (LLRLC), leaning right with left leg crossed (LRLLC), leaning back (LB), slouching (SG), shaking legs (SL). and standing (SD). These are representative of the typical sitting postures that can be found in life and work. Detailed descriptions of the typical sitting postures are shown in figure 5.

The preliminary work focused on the construction of the static posture classification system. A static posture database was established. The database contains multifarious static sitting behaviors from 10 individuals who contributed. There were 100 posture samples for each of the 12 preselected postures of the 10 participants, and each posture group of 100 samples was obtained. There was a total of 800 training sets samples, and 400 testing sets samples. The confusion matrix across all 12 classes is shown in figure 6. A static sitting posture recognition accuracy of 90.92% was achieved.

**Table 2.** Individual and overall performance values (%).

| Participant | Accuracy | Sensitivity | Specificity |
|---|---|---|---|
| 1 | 94.25 | 96.46 | 98.24 |
| 2 | 94.23 | 96.87 | 97.43 |
| 3 | 94.24 | 96.15 | 97.32 |
| 4 | 94.25 | 96.08 | 98.16 |
| 5 | 94.23 | 96.87 | 98.28 |
| 6 | 94.22 | 96.05 | 98.52 |
| 7 | 94.25 | 96.50 | 98.42 |
| 8 | 94.25 | 95.54 | 99.57 |
| 9 | 94.24 | 95.21 | 98.37 |
| 10 | 94.19 | 96.05 | 98.31 |
| Mean | 94.24 | 96.28 | 98.26 |

*4.3.2. Real-time sitting behavior recognition and rectification.* Real-time feedback and reminders to humans of sitting behavior information can improve the healthy sitting level [54–56]. Therefore, real-time sitting behavior recognition experiments were designed and implemented to test and prove the effectiveness of the RBFNN-Kernel recognition methods. The dataset containing 12 typical classes of sitting behaviors described in the preliminary work are recorded and shown in figure 6. The sitting behaviors have been recorded for three participants with similar body structures. Each wrist and shoulder joint contains three directional features, each elbow and knee joint contains four directional features, and the waist contains two directional features. Here, the 36-dimension sensor expansion directions from the data bands are used to express the sitting behaviors. Hence, the 36-dimension features were used here for sitting behavior recognition, and the training methods of the recognition models are consistent with the static sitting posture recognition models.

By looking at the analysis results in table 1, it can be seen that when compared with other methods, RBFNN-Kernel methods can achieve higher recognition accuracy for the proposed sitting behaviors. We can also see from table 1 that the RBFNN time consumed is less than that of the SVM, while the average sitting behavior recognition accuracy of RBFNN-Kernel is superior to that of the SVM. The confusion matrix of 12 sitting behaviors is shown in figure 7. We can draw the conclusion that the sitting behavior can be easily recognized according to the confusion matrices of the classifiers. Table 1 summarizes the results of the recognition accuracy for the static sitting postures, which was 94.25% for the RBFNN-Kernel methods. The RBFNN-Kernel methods achieved better recognition accuracy than the RBFNN and SVM due to the model confusion matrices.

Meanwhile, the Extended Data table 2 shows that when each data band was composed of a different number of sensors (*Nos*), the overall performance of the whole model was different, and reached the best level at the location of markings. In this table, *Nos*1 is the number of stretchable sensors on each band. *Nos*2, *Nos*3 and *Nos*4 are the number of pressure sensors of the elbow, knee, and waist bands, respectively. The conclusion can be drawn by analysis from Extended Data table 2 that when $Nos1 = 3$, $Nos2 = 2$, $Nos3 = 4$, and $Nos4 = 16$, the recognition accuracy of the sitting posture reaches the optimal level. The important physical parameters of the sensors used here are shown in Extended Data table 3.

**Table 3.** Real-time dynamic sitting behavior recognition accuracy of different approaches.

| Approaches | RBFNN-DTW | SVM-DTW |
|---|---|---|
| Accuracy (%) | 90.23 | 88.62 |

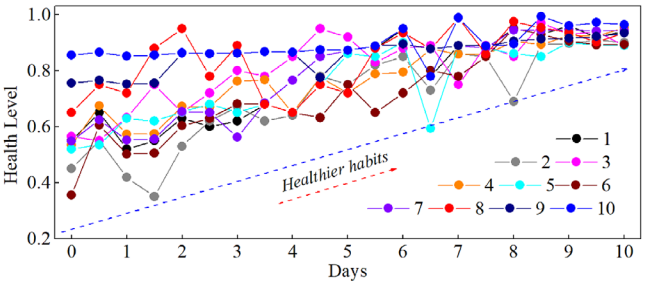


**Figure 8.** The sitting behavior health level statistics of 10 participants over 10 days.

The various age, gender, and race groups differ in height and weight [57–59]. Ten subjects (Extended Data, table 4) with different genders, ages, and weights were selected to verify the effectiveness of the proposed method, and each participant repeated the experiment three times. The leave-one-subject-out cross-validation method was adopted to estimate the generalization ability of the proposed method. Since only marked events were analyzed, there remained unlabeled samples between consecutive events. The performance values can be calculated with a timing tolerance of $\pm$ 5 samples between the labeled and estimated gait events. The conclusion can be drawn from table 2 that the performances of the proposed method do not vary with the weights and heights of the subjects. The values for each subject were obtained by averaging over all trials that the subject conducted.

The RBFNN-Kernel-DTW based method and SVM-Kernel-DTW based method are implemented to contrast their real-time sitting behavior recognition abilities using the same testing sets. The RBFNN-Kernel-DTW based technique achieved the better performance (table 3). From the confusion matrices of the classifiers in figure 7, it is concluded that the real-time sitting behavior can be easily recognized. Meanwhile, most model confusion matrices show that the RBFNN-Kernel-DTW method achieved a better recognition ability and accuracy than the SVM-Kernel-DTW based method.

Based on the proposed real-time sitting behavior tracking and recognition system, sitting habits rectification experiments were carried out. The participant in the experiment was a college student aged 22 years and weighing 60 kg and of height 170 cm, with a mild hyperactivity disorder. The experiment lasted for 5 d over a time period of 60 h, and the health levels of the sitting habits were calculated per one-hour period. The monitoring time window for each sitting behavior was set at 2 min. The statistical results of sitting habits are shown in Extended Data figure 6. The health level of the sitting posture was monitored in real time, and this information was given to the subject to remind the subject to maintain a

healthy and standard sitting posture, which will gradually improve the health level of the sitting habit. It can be concluded that from the first day to the fifth day, the health level of the sitting habit gradually increased from 33.67% to 92.50%, and the undesirable sitting behaviors were gradually rectified [60–62]. Meanwhile, the database contains multifarious sitting habits from the 10 individuals who contributed, and the sitting behavior health level statistics of 10 participants over 10 d are shown in figure 8. The experimental results of the real-time sitting behavior tracking and rectification also verify the effectiveness of the proposed methods.

## 5. Conclusion

This work involved the design of novel methods of real-time human sitting behavior tracking and recognition by means of flexible wearable data bands to ensure that the sensors were accurately attached to the joints for accurate measurement of joint movements of the shoulders, elbows, wrists, knees, and waist. The proposed fully flexible data bands are designed based on two types of flexible strain sensors. Additionally, the RBFNN-DTW-based method was used to recognize the sitting behaviors captured by the flexible wearable data bands. The proposed data bands have advantages of superior wearability and correlation of dynamic sitting behavior characteristics, compared to other wearable posture data acquisition devices. Performance evaluations verified that the proposed wearable data bands can accurately capture real-time static and dynamic sitting behaviors. Furthermore, dynamic time warping is used to select the sitting behavior candidates, with recognition being achieved by comparing an observed posture with a series of pre-recorded reference patterns, and to monitor the sitting behavior habits over a period of 10 days. Over the course of the study, through feedback reminders, the sitting habits health levels of the participants gradually increased, and the undesirable sitting behaviors were gradually rectified.

## Acknowledgments

This work was supported by the National Natural Science Foundation of China (Grant Nos. 91648206 and 61673369), the State Key Laboratory of Bioelectronics of Southeast University, the National Natural Science Foundation of China (Grant No. 61901005), and the Anhui Provincial Natural Science Foundation (Grant No. 1908085QF261).

## ORCID iDs

Yangyang Zhang https://orcid.org/0000-0003-3516-2184
Ying Huang https://orcid.org/0000-0003-4246-1895

## References

[1] Smith L *et al* 2018 Occupational physical activity habits of UK office workers: cross-sectional data from the active buildings study *Int. J. Environ. Res. Public Health* **15** 1214
[2] Fuhrer H, Kupsch A and Hälbig T D 2014 Levodopa inhibits habit-learning in Parkinson's disease *J. Neural Transm.* **121** 147–51
[3] Nooijen C *et al* 2018 Common perceived barriers and facilitators for reducing sedentary behaviour among office workers *Int. J. Environ. Res. Public Health* **15** 792
[4] Messinis G 2010 Habit formation and the theory of addiction *J. Econ. Surv.* **13** 417–42
[5] Oliver J J 2008 Cervical spondylopathy *J. Small Animal Pract.* **26** 565
[6] Mcalister C *et al* 2018 PCI following bypass graft failure is associated with poor clinical outcomes *Heart Lung Circ.* **27** S27
[7] Converse Y K, Hawkins C P and Valdez R A 2015 Habitat relationships of subadult humpback chub in the Colorado River through Grand Canyon: spatial variability and implications of flow regulation *River Res. Appl.* **14** 267–84
[8] Widjaja F F *et al* 2013 Prehypertension and hypertension among young Indonesian adults at a primary health care in a rural area *Med. J. Indonesia* **22** 39–45
[9] Pavlova A V *et al* 2014 The lumbar spine has an intrinsic shape specific to each individual that remains a characteristic throughout flexion and extension *Eur. Spine J.* **23** 26–32
[10] Danilo A *et al* 2018 Exploiting recurrent neural networks and leap motion controller for the recognition of sign language and semaphoric hand gestures *IEEE Trans. Multimedia* **21** 234–45
[11] Lu Z *et al* 2014 A hand gesture recognition framework and wearable gesture-based interaction prototype for mobile devices *IEEE Trans. Human–Mach. Syst.* **44** 293–9
[12] Wang Z *et al* 2019 Using wearable sensors to capture posture of the human lumbar spine in competitive swimming *IEEE Trans. Human–Mach. Syst.* **49** 194–205
[13] Wu Y and Huang T S 1999 Vision-based gesture recognition: a review *Int. Gesture Workshop* (Berlin: Springer) pp 103–15
[14] Chen H *et al* 2016 A review of wearable sensor systems for monitoring body movements of neonates *Sensors* **16** 2134
[15] Liu H and Wang L 2018 Gesture recognition for human-robot collaboration: A review *Int. J. Ind. Ergon.* **68** 355–67
[16] Zeng W *et al* 2014 Fiber-based wearable electronics: a review of materials, fabrication, devices, and applications *Adv. Mater.* **26** 5310–36
[17] Aggarwal J K and Xia L 2014 Human activity recognition from 3d data: a review *Pattern Recognit. Lett.* **48** 70–80
[18] Badi H S and Hussein S 2014 Hand posture and gesture recognition technology *Neural Comput. Appl.* **25** 871–8
[19] Tan C *et al* 2019 Research on gesture recognition of smart data fusion features in the IoT *Neural Comput. Appl.* **2019** 1–13
[20] Wilson A D and Bobick A F 1999 Parametric hidden Markov models for gesture recognition *IEEE Trans. Pattern Anal. Mach. Intell.* **21** 884–900
[21] Khan S, Lorenzelli L and Dahiya R S 2014 Technologies for printing sensors and electronics over large flexible substrates: a review *IEEE Sens. J.* **15** 3164–85
[22] Liu Y, Pharr M and Salvatore G A 2017 Lab-on-skin: a review of flexible and stretchable electronics for wearable health monitoring *ACS Nano* **11** 9614–35
[23] Sato J *et al* 2019 Ferroelectric polymer-based fully printed flexible strain rate sensors and their application for human motion capture *Sen. Actuators* A **295** 93–8
[24] Lu S *et al* 2019 Highly sensitive graphene platelets and multi-walled carbon nanotube-based flexible strain sensor for monitoring human joint bending *Appl. Phys.* A **125** 471
[25] Xu W 2013 Ecushion: a textile pressure sensor array design and calibration for sitting posture analysis *IEEE Sens. J.* **13** 3926–34
[26] Estrada J E and Vea L A 2016 Real-time human sitting posture detection using mobile devices *2016 IEEE Region 10 Symp.* (IEEE) pp 140–4

[27] Khan A M *et al* 2019 A triaxial accelerometer-based physical-activity recognition via augmented-signal features and a hierarchical recognizer *IEEE Trans. Inf. Technol. Biomed.* **14** 1166–72
[28] Zhu C and Sheng W 2012 Realtime recognition of complex human daily activities using human motion and location data *IEEE Trans. Biomed. Eng.* **59** 2422–30
[29] Jung P G *et al* 2015 A wearable gesture recognition device for detecting muscular activities based on air-pressure sensors *IEEE Trans. Ind. Inform.* **11** 485–94
[30] Zhu C and Sheng W 2011 Wearable sensor-based hand gesture and daily activity recognition for robot-assisted living *IEEE Trans. Syst. Man Cybern.* A **41** 569–73
[31] Van Volkinburg K and Washington G 2017 Development of a wearable controller for gesture-recognition-based applications using polyvinylidene fluoride *IEEE Trans. Biomed. Circuits Syst.* **11** 900–9
[32] Qi J *et al* 2019 Surface EMG hand gesture recognition system based on PCA and GRNN *Neural Comput. Appl.* **2019** 1–9
[33] Matsudaira P 1987 Sequence from picomole quantities of proteins electroblotted onto polyvinylidene difluoride membranes *J. Biol. Chem.* **262** 10035–8
[34] Bastas G *et al* 2018 IMU-based gait analysis in lower limb prosthesis users: comparison of step demarcation algorithms *Gait Posture* **64** 30–7
[35] Kundu A S *et al* 2017 Hand gesture recognition based omnidirectional wheelchair control using IMU and EMG sensors **91** 529–41
[36] Gao Y *et al* 2017 Acute metabolic response, energy expenditure, and EMG activity in sitting and standing *Med. Sci. Sports Exercise* **49** 1927–34
[37] Harun H, Mohd Nasir N F and Salleh A F 2016 The study of EMG signals during sitting postures in Muslim prayer *IEEE EMBS Conf. of Biomedical, Engineering and Sciences* (IEEE) pp 722–6
[38] Rajamani Y *et al* 2018 Analysis and classification of multiple hand gestures using MMG signals *J. Telecommun. Electron. Comput. Eng.* **10** 67–71
[39] Liu B *et al* 2017 Healthy human sitting posture estimation in RGB-D scenes using object context *Multimedia Tools Appl.* **76** 10721–39
[40] Zerrouki N *et al* 2018 Vision-based human action classification using adaptive boosting algorithm *IEEE Sens. J.* **18** 5115–21
[41] Plouffe G and Cretu A M 2015 Static and dynamic hand gesture recognition in depth data using dynamic time warping *IEEE Trans. Instrum. Meas.* **65** 305–16
[42] Baydogan M G, Runger G and Tuv E 2013 A bag-of-features framework to classify time series *IEEE Trans. Pattern Anal. Mach. Intell.* **35** 2796–802
[43] Kumar S and Tripathi B K 2019 On the learning machine with compensatory aggregation based neurons in quaternionic domain *J. Comput. Des. Eng.* **6** 33–48
[44] Huang Y *et al* 2018 Highly stretchable strain sensor based on polyurethane substrate using hydrogen bond-assisted laminated structure for monitoring of tiny human motions *Smart Mater. Struct.* **27** 035013
[45] Lowe D and Webb A R 1990 Exploiting prior knowledge in network optimization: an illustration from medical prognosis *Network: Computation in Neural Systems* **1** 299–323
[46] Doretto G *et al* 2003 Dynamic textures *Int. J. Comput. Vis.* **51** 91–109
[47] Yang A P *et al* 2017 Reachable domain of adults' right leg in sitting posture
[48] O'Sullivan K *et al* Can we reduce the effort of maintaining a neutral sitting posture? A pilot study *Manual Ther.* **17** 566–71
[49] Yang Y and Deng Z D 2019 Stretchable sensors for environmental monitoring *Appl. Phys. Rev.* **6** 011309
[50] Cai W *et al* 2014 Piezoresistive behavior of graphene nanoplatelets/carbon black/silicone rubber nanocomposite *J. Appl. Polym. Sci.* **131** 39778
[51] Huang Y *et al* 2019 Highly stretchable, rapid-response strain sensor based on SWCNTs/CB nanocomposites coated on rubber/latex polymer for human motion tracking *Sens. Rev.* **39** 233–45
[52] Liu P *et al* 2015 Enhanced electrical conductivity and mechanical stability of flexible pressure-sensitive GNPs/CB/SR composites: synergistic effects of GNPs and CB *J. Mater. Res.* **30** 3394–402
[53] Zhao Y *et al* 2018 Highly sensitive flexible strain sensor based on threadlike spandex substrate coating with conductive nanocomposites for wearable electronic skin *Smart Mater. Struct.*
[54] Wölfel M 2017 Acceptance of dynamic feedback to poor sitting habits by anthropomorphic objects
[55] Sengul B T 2017 A study on reading habits of social studies and history teachers in Turkey *Educ. Res. Rev.* **12** 569–82
[56] Gupta N *et al* 2017 Is questionnaire-based sitting time inaccurate and can it be improved? A cross-sectional investigation using accelerometer-based sitting time *BMJ Open* **7** e013251
[57] Lederle F A *et al* Relationship of age, gender, race, and body size to infrarenal aortic diameter *J. Vascular Surg.* **26** 595–601
[58] Rand C S W and Kuldau J M The epidemiology of obesity and self-defined weight problem in the general population: Gender, race, age, and social class *Int. J. Eating Disorders* **9** 329–43
[59] Burke G L *et al* Differences in weight gain in relation to race, gender, age and education in young adults: the CARDIA study *Ethnicity Health* **1** 327–35
[60] Herring M Y 2004 Breaking bad habits: a review essay *Libr. Cult.* **39** 452–60
[61] Ma C *et al* 2017 Posture detection based on smart cushion for wheelchair users *Sensors* **17** 719
[62] White I *et al* 2017 On Your Feet to Earn Your Seat: pilot RCT of a theory-based sedentary behaviour reduction intervention for older adults *Pilot Feasibility Studies* **3** 23